Proceedings of the Second International Conference on Press-in Engineering 2021, Kochi, Japan – Matsumoto et al (eds)

Experimental study on tsunami mitigation effect of pile-type porous tide barrier

K. Toda, A Mori & Y. Ishihara
Giken LTD, Kochi, Japan

N. Suzuki
Giken LTD, Tokyo, Japan

ABSTRACT: Damage to coastal levees and breakwaters due to the tsunami in the Great East Japan Earthquake in 2011 have brought up issues on the necessity of improving the tenacity of these structures. Use of piles in these structures will be effective in enhancing their tenacity. Among several possibilities in structural types of these structures with piles, a pile-type porous tide barrier is expected to be helpful in reducing the tsunami load that passes through it and preventing the existing structures from collapsing. This paper introduces model tests examining the effect of the pile-type porous tide barrier in reducing the surge-type tsunami load. Based on several test results with different porosity ratios and a theoretical approach to interpret the experimental data, it was found that the tsunami mitigation effect of the barrier can be captured by loss factor, which can be defined by combining the porosity ratio and the friction factor.

1 INTRODUCTION

Damage to coastal levees and breakwaters due to the tsunami in the Great East Japan Earthquake in 2011 have brought up issues on the necessity of improving the tenacity of these structures (MLIT, 2013). Use of piles in these structures will be effective in enhancing their tenacity. For example, Kikuchi *et al.* (2015) confirmed the effectiveness of reinforcing the gravity-type breakwater using pipe piles. Suzuki *et al.* (2016a) investigated the effect of the breakwater consisting of arrays of steel tubular piles to mitigate the tsunami load, and proposed its design method through a theoretical approach. In addition to these structures with piles, a pile-type porous tide barrier (hereinafter called as "Implant Barrier" or "Barrier") is expected to serve as one of the countermeasures against tsunami.

The basic structure of the Implant Barrier is shown in Figure 1. It consists of columns, (steel tubular piles), porous sheets (fabric materials) and sheet piles (optionally). The columns are aligned with a certain distance between themselves, and are embedded into the ground to generate enough horizontal resistance to secure the structural stability of the Barrier. The porous sheets are supposed to be made of fabric materials and are fixed to the columns, and have a function of inducing an energy loss of the tsunami when it passes through them. The porosity ratio of the porous sheet is expressed as Equation (1), and the porosity ratio of the Barrier is defined by Equation (2).

$$\lambda = A_P/(L_P H) \tag{1}$$

$$\lambda_B = L_P \lambda / L_C \tag{2}$$

where H is the height of the Barrier, D_C is the outer diameter of the column, L_C is the distance between two adjacent columns, L_P is the horizontal length of one porous sheet between two columns and A_P is the area of the porous parts in one porous sheet between two columns, as illustrated in Figure 2. Sheet piles are expected to be optionally used to ensure the stability of the Barrier by avoiding the deformation of the ground surface due to erosion, seepage failure, liquefaction and so on. With the above-mentioned structure, the Barrier is expected to be effective in reducing the load of tsunami that passes through it and preventing the existing structures behind the Barrier from collapsing.

The effect of the Barrier on reducing the tsunami load has partly been investigated so far. Suzuki *et al.* (2016b) provided a theoretical approach to explain the load, velocity and the height of tsunami in front of and behind the Barrier, and confirmed its validity through a series of two-dimensional hydraulic model tests by using a surge-type tsunami. However, in their model tests, the tsunami load was not measured behind the Barrier, and the tsunami mitigation effect of the Barrier was captured by the water depth behind

DOI: 10.1201/9781003215226-44

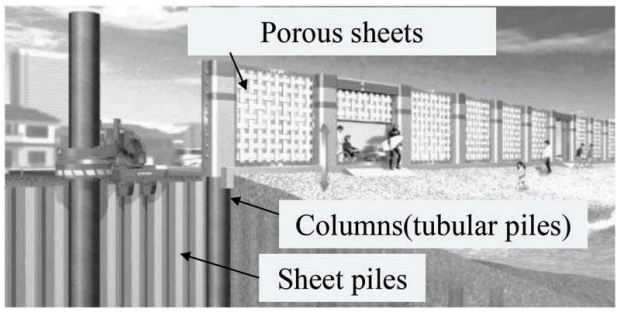

Figure 1. Basic structure of the Barrier.

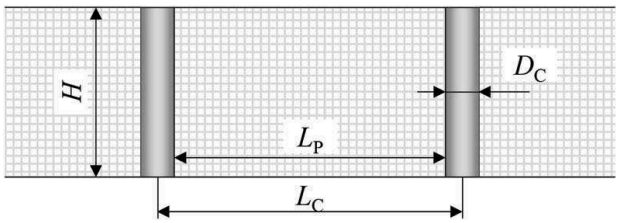

Figure 2. Parameters related to the geometry of the Barrier.

the Barrier. It is necessary to measure the tsunami load behind the Barrier to understand more directly the effect of the Barrier on reducing the tsunami load. Furthermore, the applicability of the theoretical approach to the condition where the height of tsunami exceeds the Barrier has not been investigated, although a tsunami with such a height was dealt with in their model tests. In order to expand the applicability of the Barrier, it is necessary to investigate the applicability of the theoretical approach to such a condition.

This paper reports the results of the two-dimensional hydraulic model tests on the Barrier, where the load of a surge-type tsunami behind the Barrier was measured. In addition, based on the test results, the applicability of the theoretical approach to tsunami higher than the Barrier is studied.

2 MODEL TESTS

2.1 *Apparatus*

The model tests were conducted using an experimental facility called Tsunami Simulator in Giken (Figure 3). The apparatus consists of a surface tank for storing water, a gate, a channel and an underground tank for storing water. The channel has a length of 19.5 m, a width of 1.5 m and a depth of 0.8 m. Details of this apparatus can be found in Ishihara *et al*. (2018).

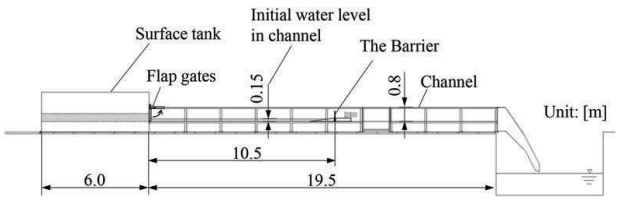

Figure 3. Experimental apparatus (Tsunami Simulator).

In this research, a surge-type model tsunami, simulating the front part of tsunamis, were generated by accumulating water in the surface tank and opening the gate instantaneously.

The layout of the test is shown in Figure 4. A slope of 1/7 was placed on the floor of the channel to simulate a geographical feature of coastal areas, and the model of the Barrier was fixed at the end of the slope with the distance from the gate being 10.5 m. The height of the end of the slope was 0.2 m from the floor of the channel, and the initial water level was set as 0.15 m. The height of the Barrier was 0.35 m (i.e. the head of the barrier was 0.55 m above the floor of the channel).

The columns of the Barrier were modelled by polyvinyl chloride pipes with the outer diameter of 48 mm. The scaling law was ignored in terms of their cross-sectional performance (flexural rigidity), as the deformation of the columns were out of scope of this research. The porous sheets were modelled by the glass cloths. The upper and lower edges of the glass cloths were protected by plastic tapes to avoid their fray, as shown in Figure 5.

The layout of measurement is shown in Figure 6. Flow velocimeters and wave gauges were settled at three positions: “Upstream” which was 2000 mm in front of the Barrier, “Front” which was 75 mm in front of the Barrier and “Downstream” which was 490 mm behind the Barrier. The tsunami load on the Barrier was obtained by the readings of the load cells equipped in the lower part of the columns of the Barrier. The load of tsunami that passed through the Barrier was measured by the load measuring device just behind the “Downstream” position as shown in Figure 7, where strain gauges were attached on steel parts which were

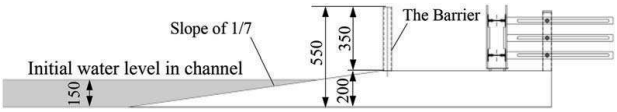

Figure 4. Test layout in “To” test series.

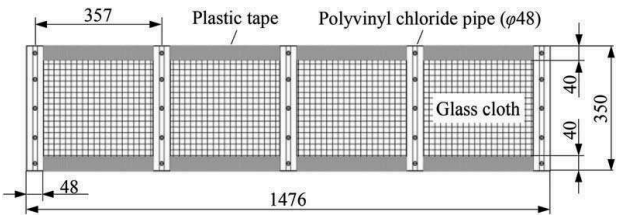

Figure 5. Protection of the upper and lower edges of the model porous sheets.

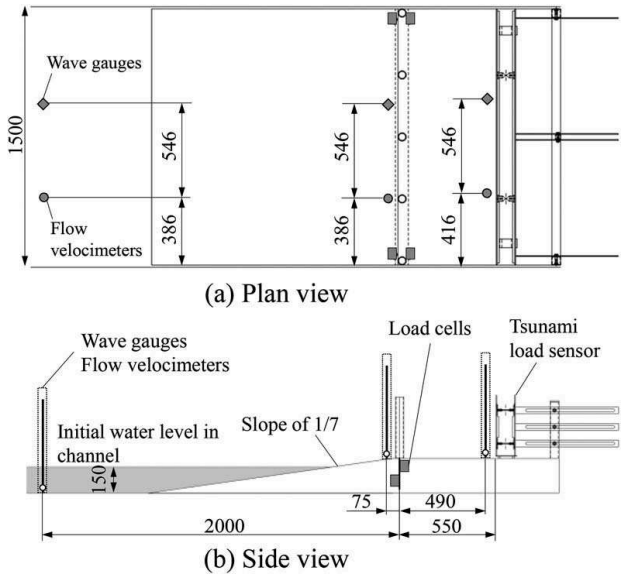

Figure 6. Layout of measurement in "To" test series. (a) Plan view (b) Side view.

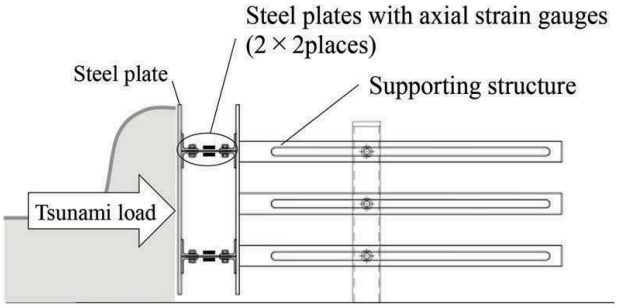

Figure 7. Tsunami load measuring device placed near the "Downstream" position.

fixed to the steel plate facing tsunami and the supporting structure that was fixed to the floor.

2.2 *Test cases*

A total of 8 tests were newly conducted as shown in Table 1, to compare the effect of the Barrier on reducing the tsunami load. Four different tests were conducted twice. Cases To-1, To-2 and To-3 were conducted with the measurement of the tsunami load behind the Barrier, while Case To-4 was conducted without the measurement of the tsunami load behind the Barrier to allow a direct comparison with the test results of Suzuki *et al*. (2016b).

Case To-1 was conducted without the Barrier, while Cases To-2, To-3 and To-4 were conducted with the Barrier. Figure 8 shows the shape of the Barrier was flat in Cases To-2 and To-4, and was

Table 1. Test conditions in "To" test series.

No.	Material of porous sheets	Porority ratio	Shape of the Barrier	Measurement of tsunami load behind the Barrier
To-1(1)	-	100%	-	Conducted
To-1(2)	-	100%	-	Conducted
To-2(1)	Glass cloth (#110)	24%	Flat	Conducted
To-2(2)	Glass cloth (#110)	24%	Flat	Conducted
To-3(1)	Glass cloth (#220)	24%	Flexure	Conducted
To-3(2)	Glass cloth (#220)	24%	Flexure	Conducted
To-4(1)	Glass cloth (#110)	24%	Flat	Ommitted
To-4(2)	Glass cloth (#110)	24%	Flat	Ommitted

flexure in Case To-3. The porosity ratio of the porous sheets in Case To-3 was smaller than that in Cases To-2 and To-4, so that the porosity ratio of the Barrier was comparable in these test cases. It should be noted that the tsunami load on the Barrier was not measured in Case To-3, because the bottom of each porous sheet was fixed to the floor with tapes in order to prevent tsunami from leaking and to maintain the flexural shape of the porous sheet.

2.3 *Results*

Regarding the effect of the Barrier on mitigating the tsunami load, Figure 9 shows the variation of the flow velocity and the water depth at the "Downstream" position with time (t), as well as that of the tsunami load measured just behind the "Downstream" position. The origin of the horizontal axis was taken as the time when the tsunami arrived at the "Upstream" position.

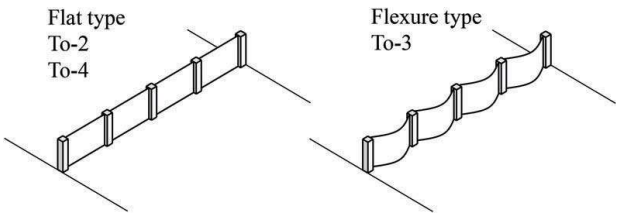

Figure 8. Shape of the Barrier.

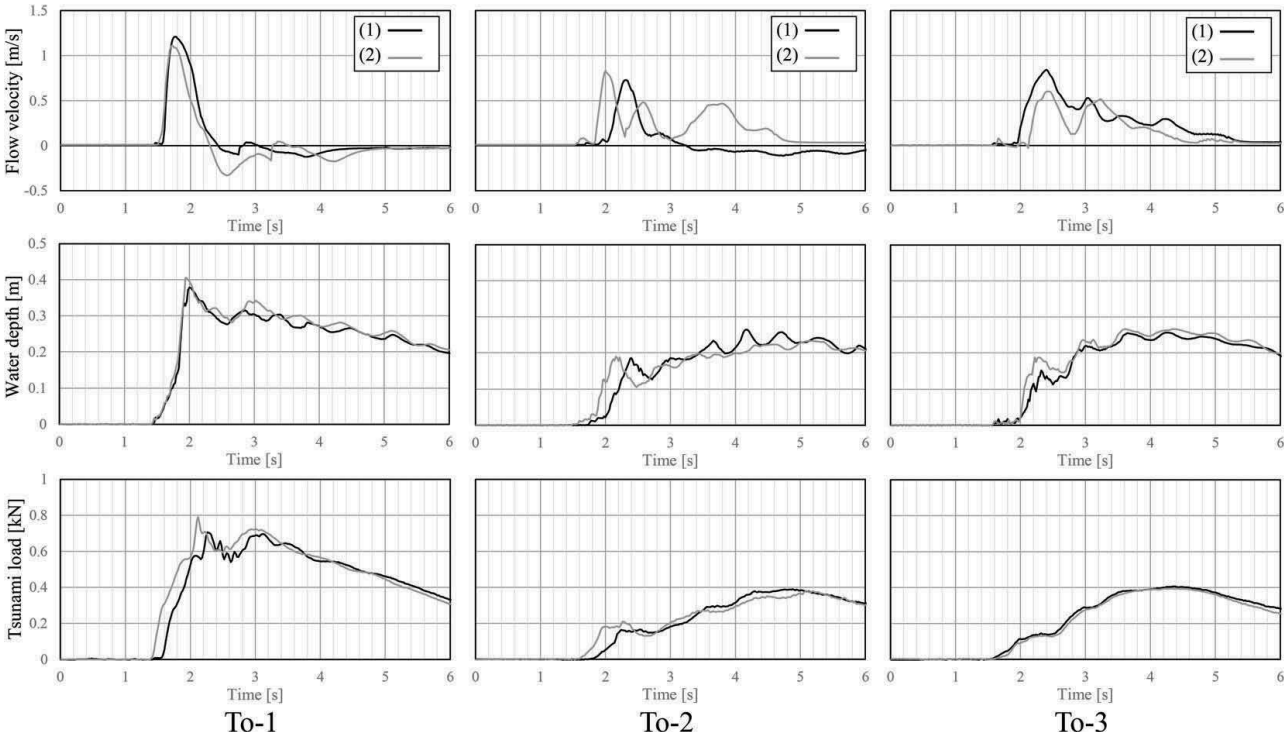

Figure 9. Time-series data of flow velocity and water depth at the "Downstream" position.

The water depth started to increase when t was around 1.5 s and arrived its local peak when 2.0 s < t < 2.5 s. After that, it gradually decreased in Case To-1 (without Barrier), while it kept increasing in Cases To-2 and To-3 (with Barrier) and reached its peak when 4.0 s < t < 5.0 s. This might be because, as illustrated in Figure 10, the tsunami reflected at the tsunami load measuring device was again reflected at the Barrier in Cases To-2 and To-3, and more amount of water was captured in between the Barrier and the tsunami load measuring device.

The flow velocity started to increase when t was around 1.5 s and arrived its peak by the time when t increased to 2.5 s. After that, it sharply decreased to zero or negative values in Case To-1 (without Barrier) while it gradually decreased in Cases To-2 and To-3 (with Barrier).

Regarding the tsunami load, the trend of variation with time was more similar to that of the water depth rather than that of the flow velocity. It started to increase when t was around 1.5 s, arrived its local peak when 2.0 s < t < 2.5 s, and then gradually decreased in Case To-1 (without Barrier) while it kept increasing in Cases To-2 and To-3 (with Barrier) and reached its peak when 4.0 s < t < 5.0 s.

The above-mentioned trends of the water depth, flow velocity and tsunami load after the initial local peak will be influenced by the duration of the tsunami, and will better be dealt with by the experiments using a reflux-type model tsunami (i.e. a continuous flow). As the experiment in this paper uses the surge-type tsunami with a limited duration, the discussion hereinafter will be made by focusing on the measured values in t < 2.5 s.

Comparing To-1 and To-2, the Barrier with a flat shape reduced the water depth, flow velocity and the tsunami load at or near the "Downstream" position by 33%, 52% and 75% respectively, which demonstrates the effectiveness of the Barrier on reducing the tsunami load. In addition, comparing To-1 and To-3, the Barrier with a flexural shape reduced the water depth, flow velocity and the tsunami load at or near the "Downstream" position by 38%, 57% and 80% respectively. The Barrier with a flexural shape provided additional effect of reducing the tsunami load. It is suggested that this was because the flexural shape of the porous sheets was effective in changing the direction of the flow behind the Barrier, leading to a collision of each flow and the loss of its energy as shown in Figure 11.

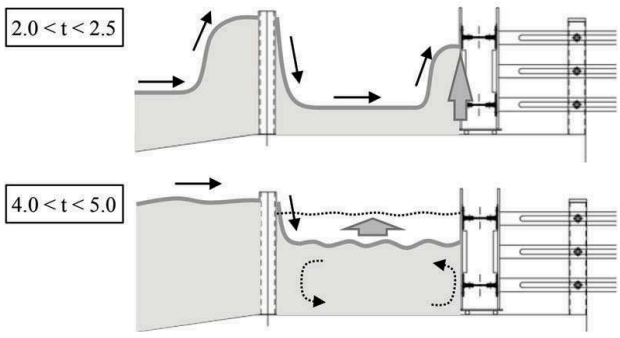

Figure 10. Inferred mechanism of the water depth increase behind the Barrier.

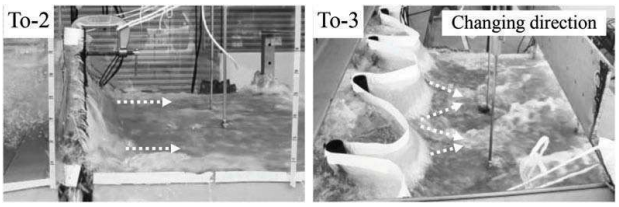

Figure 11. Inferred mechanism of the additional effect of flexural porous sheets.

3 THEORETICAL APPROACH OF DESIGNING THE BARRIER

3.1 *Surge-type tsunami not overflowing the Barrier*

3.1.1 *Basic theory*

As proposed by Suzuki *et al.* (2016b), a situation where the Barrier is fixed to a flat ground and the tsunami is flowing through the Barrier without overflowing it is considered, as shown in Figure 12. The subscripts U, F and D of the parameters represent the positions of "Upstream", "Front" and "Downstream" respectively.

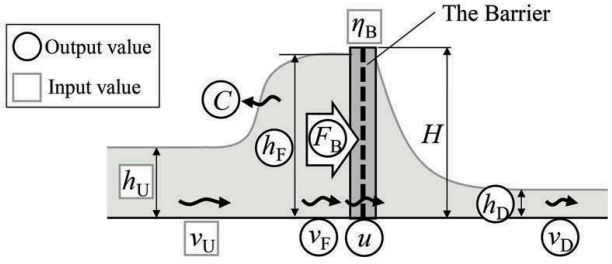

B	[m]	: Width of the channel
H	[m]	: Height of the Barrier
C	[m/s]	: Velocity of the flow reflected by the Barrier
F_B	[kN]	: Tsunami load on the Barrier
f		: Friction factor
g	[m/s^2]	: Gravitational acceleration
h_U	[m]	: Water depth at "Upstream" position
h_F	[m]	: Water depth at "Front" position
h_D	[m]	: Water depth at "Downstream" position
v_U	[m/s]	: Flow velocity at "Upstream" position
v_F	[m/s]	: Flow velocity at "Front" position
v_D	[m/s]	: Flow velocity at "Downstream" position
u	[m/s]	: Velocity of the flow in the porous parts of the Barrier
η		: Loss factor of the porous sheet
η_B		: Loss factor of the Barrier
λ		: Porosity ratio of the porous sheet
λ_B		: Porosity ratio of the Barrier
ρ	[t/m^3]	: Density of water

Figure 12. Model considered in the theoretical approach.

C [m/s] : Velocity of the flow reflected by the Barrier
F_B [kN] : Tsunami load on the Barrier
f : Friction factor
g [m/s^2] : Gravitational acceleration
h_U [m] : Water depth at "Upstream" position
h_F [m] : Water depth at "Front" position
h_D [m] : Water depth at "Downstream" position
v_U [m/s] : Flow velocity at "Upstream" position
v_F [m/s] : Flow velocity at "Front" position
v_D [m/s] : Flow velocity at "Downstream" position
u [m/s] : Velocity of the flow in the porous parts of the Barrier
η : Loss factor of the porous sheet
η_B : Loss factor of the Barrier
λ : Porosity ratio of the porous sheet
λ_B : Porosity ratio of the Barrier
ρ [t/m^3] : Density of water

Based on the continuity of the flowrate around the Barrier,

$$Q = Bv_F h_F = Bv_D h_D \tag{3}$$

Considering the law of conservation of momentum around the Barrier, the tsunami load on the Barrier (F_B) is expressed as:

$$F_B = \frac{1}{2}\rho g B\left(h_F{}^2 - h_D{}^2\right) + \rho B\left(h_F v_F{}^2 - h_D v_D{}^2\right) \tag{4}$$

Assuming that the energy loss around the Barrier is caused only by the transmission of the flow in the porous parts, the law of conservation of energy around the Barrier can be written as:

$$f\frac{1}{2g}u^2 = \left(\frac{1}{2g}v_F{}^2 + h_F\right) - \left(\frac{1}{2g}v_D{}^2 + h_D\right) \tag{5}$$

Based on the continuity of the flowrate,

$$u = v_F/\lambda \tag{6}$$

Combining Equations (5) and (6),

$$\frac{1}{2g}\frac{f}{\lambda^2}v_F{}^2 = \frac{1}{2g}\left(v_F{}^2 - v_D{}^2\right) + \left(h_F - h_D\right) \tag{7}$$

On the other hand, from a coordinate system that travels inversely to the tsunami at the velocity of C, the continuity of flowrate and the conservation of momentum at "Downstream" and "Front" positions can be expressed as:

$$B\ (v_F+C)h_F = B(v_U+C)h_U \tag{8}$$

$$\frac{1}{2}\rho g B {h_F}^2+\rho B h_F(v_F+C)^2=\frac{1}{2}\rho g B {h_U}^2+\rho B h_U(v_U+C)^2 \tag{9}$$

Based on the experimental results of Suzuki *et al.* (2016b), the flow velocity of the tsunami may be assumed as being independent of the existence of the Barrier.

$$v_D = v_U \tag{10}$$

By the way, it is complicated from a practical point of view to obtain both the porosity ratio (λ) and the friction factor (f) when designing the Barrier. In addition, it is difficult to obtain an accurate value of λ for a porous sheet with a complicated structure (e.g. a fabric sheet consisting of a lot of strings). To cope with these difficulties, a parameter called "loss factor" (η), as expressed by Equation (11), will be introduced.

$$\eta = \frac{f}{\lambda^2} \tag{11}$$

As a method to obtain the loss factor (η), the following experimental method will be introduced, by consulting the method of Hasegawa *et al.* (1987). As shown in Figure 13, two PVC (polyvinyl chloride) pipes with flanges are prepared, and the porous sheet is sandwiched between the two flanges. While maintaining a steady flow inside the pipe, the water pressures are measured at both sides of the porous sheet, and the flowrate is measured by an ultrasonic flowmeter in the downstream side. The loss factor is obtained by:

$$\eta = \frac{2\Delta p}{\rho v^2} \tag{12}$$

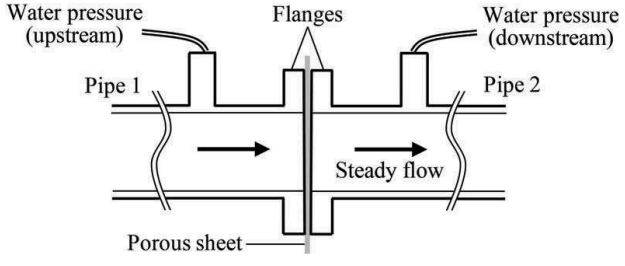

Figure 13. Experimental method to obtain the loss factor.

where Δp is the difference of the water pressure at the two measurement positions and v is the flow velocity calculated from the measured flowrate.

Precisely speaking, the porosity ratio and the loss factor of the Barrier (λ_B and η_B) are different from those of the porous sheets (λ and η) due to the existence of the tubular piles with its porosity ratio being zero. η_B would be assumed to be obtained by:

$$\eta_B = \frac{\lambda^2}{{\lambda_B}^2}\eta \tag{13}$$

Plugging Equations (11) into Equation (7), and replacing η by η_B, Equation (14) is reduced to:

$$\eta_B \frac{1}{2g}{v_F}^2 = \frac{1}{2g}\left({v_F}^2 - {v_D}^2\right)+(h_F - h_D) \tag{14}$$

Equations (3), (4), (8), (9), (10) and (14), which consist of 9 parameters (C, F_B, h_U, h_F, h_D, v_U, v_F, v_D, η_B), can be solved by considering the input values for h_U, v_U and η_B, to obtain the values of the other 6 parameters.

3.1.2 *Verification of the theoretical approach by comparing with model test results*

The conditions and the results of the model tests conducted by Suzuki *et al.* (2016b) and those introduced in Section 2 are summarized in Table 2. The values of the tsunami load on the Barrier are the initial local peak values, and the values of the water depth at the "Front" position are those recorded at the same timing (when the tsunami load on the Barrier arrived at the initial local peak values). The values of the water depth at the "Downstream" position are the initial local peak values. Note that a slight overflowing was observed in Case Su-6 (with 0% porosity ratio).

The input values for the three parameters (h_U, v_U and η_B) are summarized in Table 3. Regarding h_U and v_U, the values recorded at the "Upstream" position without the Barrier were adopted. The values of η_B were obtained experimentally based on the method introduced in Section 3.1.1. By applying the steady flow with its flow velocity being varied up to the value adopted in the model tests in Suzuki *et al.* (2016b) and in Section 2, η was confirmed to be little influenced by v. In this research, η was taken as the average of the measured values when v was in between 0.6 and 0.8 m/s. The obtained values of η are shown in Table 2, and the values of η_B obtained by Equation (13) are shown in Table 3. Note that the η_B values in the test cases with 100 % porosity (i.e. without the Barrier) and with 0 % porosity were taken as 0.1 and 10000 respectively to be plotted on log-scale graphs, although they are supposed to be 0 and ∞ theoretically.

Table 2. Test conditions and results (surge-type tsunami not overflowing the Barrier).

Case No.	Porous material	Porority ratio λ	Porority ratio λ_B	Loss factor* η	Water depth at "Front" h_F[m]	Tsunami load on the Barrier F_B[kN]	Water depth at "Downstream" h_D[m]	Remarks
Su-1	-	100%	100%	0.1	0.155	0.025	0.118	Suzuki etal. (2016b)
Su-2	Punching metal	33%	33%	6	0.295	0.386	0.064	
Su-3	Punching metal	10	10	147	0.347	0.557	0.021	
Su-4	Grass cloth	40%	40%	14	0.225	0.421	0.031	
Su-5	Grass cloth	10%	10%	353	0.342	0.612	0.037	
Su-6	Steel plate	0%	0%	10000	0.351	0.787	0.027**	
To-4(1)		40%	24%	14	0.346	0.348	0.042	This report
To-4(2)					0.333	0.344	0.046	

* Suzuki etal., 2016b. ** Overflow.

Table 3. Input values for designing the Barrier not overflown by tsunami.

Case No.	Flow velocity v_U [m/s]	Water depth h_U [m]	Loss factor η_B
Su-1	1.28※	0.155※	0.1
Su-2			6
Su-3			147
Su-4			14
Su-5			353
Su-6			10000
To-4(1)	1.27	0.162	39
To-4(2)			

Figure 14 shows the comparison of the water depth at the "Front" position (h_F), tsunami load on the Barrier (F_B) and the water depth at the "Downstream" position (h_D) measured in the model tests and estimated by the theoretical approach. The input values for the estimation are shown in Table 3. Good agreement between the measured and estimated values is confirmed for the three parameters.

3.2 *Surge-type tsunami overflowing the Barrier*

3.2.1 *Introduction of equivalent porosity ratio and equivalent loss factor of the Barrier*

To apply the theoretical approach in Section 3.1 to the cases where the Barrier is overflown by the tsunami, an imaginary Barrier that has the same height with the tsunami will be considered, and the concept of the equivalent porosity ratio of the Barrier (λ_B') and the equivalent loss factor of the Barrier (η_B') will be introduced. As illustrated in Figure 15, λ_B' will be obtained by averaging the porosity ratio of the actual Barrier above its actual height (= 0%) and that below its actual height (= λ_B) over the height of the imaginary Barrier, as expressed by:

$$\lambda_B' = \frac{1\times(h_F - H)+\lambda_B H}{h_F} = 1 - \frac{H}{h_F}(1-\lambda_B) \quad (15)$$

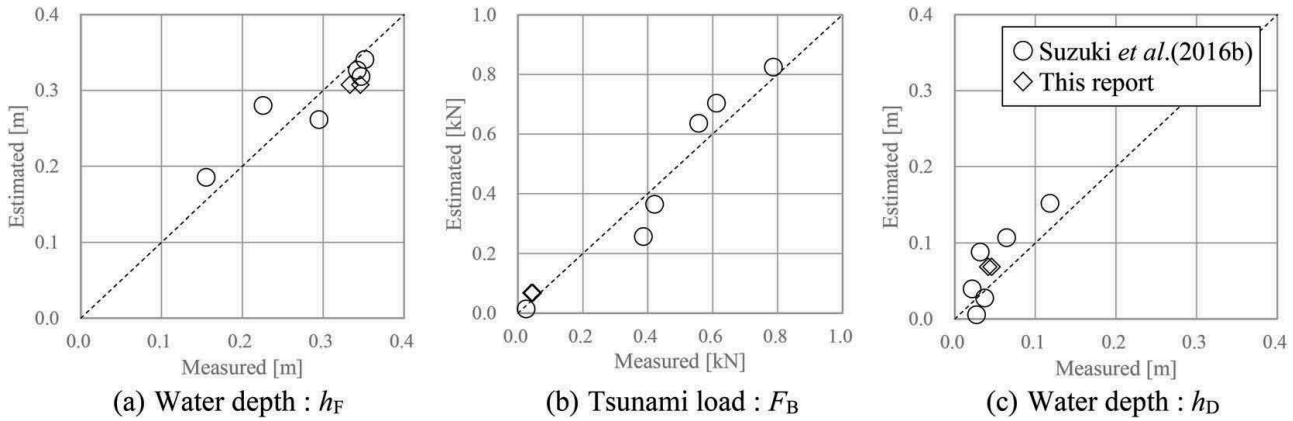

Figure 14. Comparison of measured and estimated results (with tsunami not overflowing the Barrier).

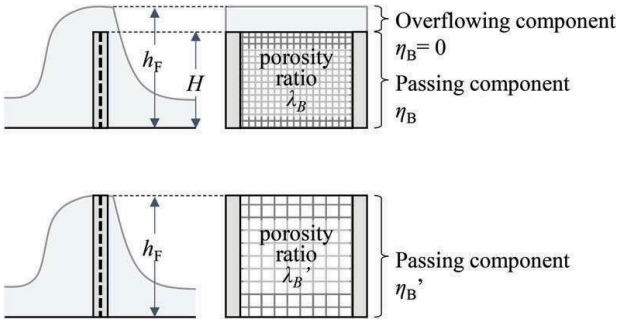

Figure 15. Correction of porosity ratio when tsunami overflows the Barrier.

Table 5. Input values for designing the Barrier overflown by tsunami.

Case No.	Flow velocity v_U [m/s]	Water depth h_U [m]	Loss factor* η_B	Corrected Loss factor η_B'
Su-1	1.36※	0.189※	0.1	0
Su-2			6	6
Su-3			147	48
Su-4			14	14
Su-5			353	88
Su-6			10000	76

*Suzuki et al., 2016b

Replacing λ_B and η_B in Equation (13) by λ_B' and η_B', η_B' is expressed as:

$$\eta_B' = \frac{\lambda_B^2}{\lambda_B'^2}\eta_B = \eta_B \frac{\lambda^2}{\left(1 - \frac{H}{h_F}(1 - \lambda_B)\right)^2} \quad (16)$$

Adopting λ_B' and η_B' obtained by Equations (15) and (16) instead of λ_B and η_B in Equations (3), (4), (8), (9), (10) and (14), along with the input values for h_U, v_U and η_B', the values of the other 6 parameters (C, F_B, h_F, h_D, v_F, v_D) can be obtained.

3.2.2 *Comparison with the model test results*

The conditions and the results of the model tests conducted by Suzuki *et al.* (2016b), where tsunamis overflew the Barrier, are summarized in Table 4. Figure 16 shows the comparison of the water depth at the "Front" position (h_F), tsunami load on the Barrier (F_B) and the water depth at the "Downstream" position (h_D) measured in the model tests and estimated by the theoretical approach based on the input values shown in Table 5. Regarding h_D, a good agreement can be found, with a slight overestimating tendency (which leads to a slightly conservative design). On the other hand, h_F and F_B were underestimated. This might be partly because the instant increase of the water depth in front of the Barrier just after it was hit by the tsunami is not considered in the theoretical approach.

To cope with the underestimating tendency of h_F and F_B under the condition of tsunami overflowing the Barrier, it was attempted to obtain the corrected water depth (h_{F_o}) based on the correlation between the estimated and measured h_F. Considering the trend line obtained by the least-square method as shown in Figure 16(a), h_{F_o} is expressed as:

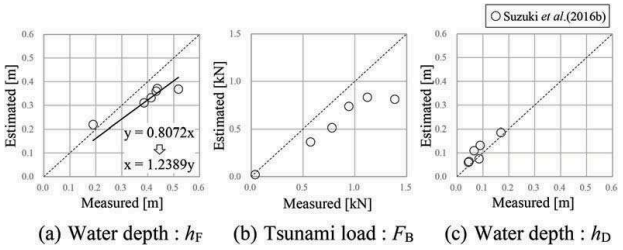

(a) Water depth : h_F (b) Tsunami load : F_B (c) Water depth : h_D

Figure 16. Comparison of measured and estimated results (with tsunami overflowing the Barrier).

Table 4. Test conditions and results (surge-type tsunami overflowing the Barrier).

Case No.	Porous material	Porority ratio λ	Porority ratio λ_B	Loss factor* η	Water depth at "Front" h_F[m]	Tsunami load on the Barrier F_B[kN]	Water depth at "Downstream" h_D[m]	Remarks
Su-1	-	100%	100%	0.1	0.189	0.037	0.169	Suzuki et al. (2016b)
Su-2	Punching metal	33%	33%	6	0.385	0.572	0.089	
Su-3	Punching metal	10	10	147	0.432	0.942	0.085	
Su-4	Grass cloth	40%	40%	14	0.412	0.778	0.066	
Su-5	Grass cloth	10%	10%	353	0.436	1.120	0.044	
Su-6	Steel plate	0%	0%	10000	0.518	1.384	0.046	

*Suzuki et al., 2016b.

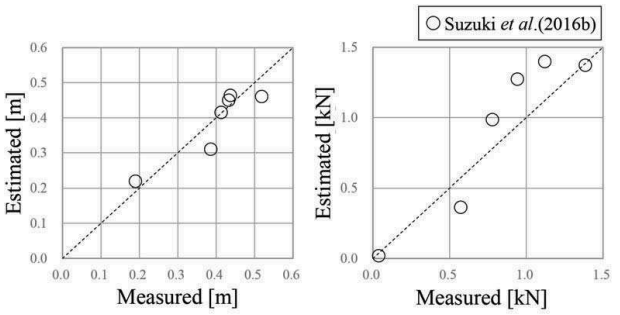

Figure 17. Comparison of measured and estimated results (with tsunami overflowing the Barrier, with corrected hF in estimation).

$$h_{F\_o} = 1.25 h_F \tag{17}$$

Substituting Equation (17) into Equation (4), the corrected tsunami load on the Barrier (F_{B_o}) is obtained by:

$$F_{B\_o} = \frac{1}{2}\rho g B\left(h_{F\_o}{}^2 - h_D{}^2\right) + \rho B\left(h_{F\_o} v_F{}^2 - h_D v_D{}^2\right) \tag{18}$$

The corrected water depth and tsunami load were compared with the measured water depth and tsunami load, as shown in Figure 17. The underestimating trends were mitigated.

The above correction was based on the test result and is empirical. It is a future work to generalize the method of correcting the water depth in front of the Barrier. In addition, it is unknown if the theoretical approach in this paper is directly applicable to the cases where the slope angle of the ground is different from that in the model tests in this research (= 1/7), as it is conjectured that the increase in the water depth in front of the Barrier might be greater if the slope angle of the ground becomes smaller.

4 SCALE EFFECT ON THE LOSS FACTOR

In this section, the scale effect on the loss factor is briefly discussed, to confirm the possibility of expanding the findings in this research to actual (full-scale) projects.

According to several researches on the pressure loss when a fluid passes through small apertures (Hamaguchi *et al.*, 1982; Hasegawa *et al.*, 1987), the friction factor (f) becomes constant if the Reynolds number (R_e) obtained by Equation (19) is greater than 500.

$$R_e = \frac{lu}{\nu} \tag{19}$$

Here, l is the representative length (the size of a small aperture or the porous part of the Barrier), u is the flow velocity of a liquid in the small apertures and v is the coefficient of kinematic viscosity of the liquid.

Table 6 shows the values of l, u and R_e in the model tests introduced in this paper, where l was taken as the aperture of the porous part of the Barrier and u was obtained by Equation (6) using the flow velocity (v_F) recorded when the tsunami load on the

Table 6. Values of Reynolds number in the model tests.

Case No.	Over flow	Porority ratio λ	Aperture width l[mm]	Flow velocity v_F[m/s]	Flow velocity u^*[m/s]	Reynolds number R_e
Su-1	No	100%	-	1.277	-	-
Su-2	No	33%	3.0	1.045	3.167	9502
Su-3	No	10	4.0	0.738	7.377	29507
Su-4	No	40%	0.8	0.013	2.533	2027
Su-5	No	10%	1.2	0.666	6.656	7987
Su-6	No	0%	-	0.611	-	-
To-4(1)		24%	0.8	0.611	2.554	2035
To-4(2)			0.8	0.611	2.554	2043
Su-1	Yes	100%	-	1.368	-	-
Su-2	Yes	33%	3.0	0.765	2.319	6958
Su-3	Yes	10	4.0	0.302	3.023	12092
Su-4	Yes	40%	0.8	0.703	1.758	1407
Su-5	Yes	10%	1.2	0.446	4.463	5356
Su-6	Yes	0%	-	0.330	-	-

* $u = v_F/\lambda$ (Suzuki et al., 2016b)
Dynamic viscosity coefficient of water: $\nu = 0.000001$ [m^2/s]

Barrier (F_B) increased to its initial local peak. The value of ν was taken as 1.0 x 10^{-6} m/s. It can be confirmed that the R_e values in the model tests exceeded 500, which would be suggesting that the scale effect on the loss factor can be ignored in this model test and the findings in this paper can be applied to the full-scale prototype.

When designing the prototype Barrier based on the methods in this paper, it is desirable to obtain the value of the loss factor (η) of the porous sheet by conducting the experiment introduced in Section 3.1.1 under the condition of the R_e value controlled similar to that in the prototype (desirably by using the actual porous sheet). Even if this is difficult, it is necessary to confirm that the R_e values of the prototype and the experiment are greater than 500.

5 CONCLUSIONS

Results of the two-dimensional hydraulic model tests on the Barrier, where the load of a surge-type tsunami behind the Barrier was measured, were reported. The Barrier with the porosity ratio of 24 % was confirmed to reduce the tsunami load behind the Barrier by 75% if the porous sheet was flat and by 80% if the porous sheet was flexural.

A theoretical approach to design the Barrier, based on a model where the Barrier is placed on a flat ground and the tsunami flows without overflowing it, as proposed by Suzuki *et al*. (2016b), was explained. In this theoretical approach, the loss factor was introduced to simplify the design process. An experimental method to obtain the loss factor was also introduced. This theoretical approach was then expanded to be applied to the condition where the tsunami overflows the Barrier, by introducing the equivalent porosity ratio and the equivalent loss factor.

The validity of the theoretical approaches was confirmed by comparing with the results of the model tests newly introduced in this paper as well as those conducted by Suzuki *et al*. (2016b). As a result, good agreement between the estimated and measured values of the water depth in front of and behind the Barrier and the tsunami load on the Barrier was confirmed for the cases with the tsunami not overflowing the Barrier. On the other hand, for the cases where the tsunami overflowed the Barrier, good agreement between the estimated and measured values of the water depth behind the Barrier was confirmed, while the water depth in front of the Barrier and the tsunami load on the Barrer were underestimated. It was confirmed that these underestimating trends were mitigated if the water depth in front of the Barrier was corrected based on the model test results.

The scale effect on the loss factor was discussed, and it was suggested that the theoretical approach in this paper would be applied to designing the prototype scale Barrier if the porous sheet was selected so that the Reynolds number become greater than 500.

Further research is necessary to investigate the applicability of the theoretical approach to the cases where the Barrier is placed on the ground with its slope angle being different from that in the model tests in this research (= 1/7). In addition, additional model tests are necessary to investigate the effectiveness of the Barrier under the steady flow (i.e. a tsunami with a long wave length).

REFERENCES

Hamaguchi, K., Takahashi, S. and Miyabe, H. 1982. Flow losses of regenerator matrix: case of packed wire gauges. *Transactions of the Japan Society of Mechanical En-gineers, Series B*, Vol. 48, No. 435: 2207–2216. (in Japanese)

Hasegawa, T., Fukutomi, K., Narumi, T. 1987. A study of a flow through small apertures (1st report, Experiments on the excess pressure drop). *Transactions of the JSME, Series B*, Vol.53, No.496: 3510–3515. (in Japanese)

Ishihara, Y., Okada, K. and Hamada, M. 2018. Comparison of pile-type and gravity-type coastal levees in terms of resilience to tsunami. Proceedings of the First International Conference on Press-in Engineering 2018, Kochi: 251–256.

Kikuchi, Y., Kawabe, S., Taenaka, S. and Moriyasu, S. 2015. Horizontal loading experiments on reinforced gravity type breakwater with steel walls. *The 15th Asian Regional Conference on Soil Mechanics and Geotechnical Engineering, Japanese Geotechnical Society Special Publication*, Vol. 2, Issue 35: 1267–1272.

Ministry of Land, Infrastructure, Transport and Tourism (MLIT). 2013. Guideline for Tsunami-Resistant Design of Seawall (Parapet Wall): 18p.

Suzuki, N., Ishihara, Y. and Isobe, M. 2016a. Experimental study on tsunami mitigation effect of breakwater with arrays of steel tubular piles. *Journal of Social Safety Science*, No. 29, 2016.11: 7–14. (in Japanese)

Suzuki, N., Ishihara, Y., Isobe, M. 2016b. Experimental study on influence of porosity and material of Pile-type porous tide barrier on its tsunami mitigation effect. *Journal of Japan Society of Civil Engineers. Ser. B3 (Ocean Engineering)*: I_491-I_496. (in Japanese)